

Improvement of Snow Gauge Collection Efficiency through a Knowledge of Solid Precipitation Fall Speed

NICOLAS R. LEROUX,^a JULIE M. THÉRIAULT,^a AND ROY RASMUSSEN^b

^a Centre ESCER, Department of Earth and Atmospheric Sciences, Université du Québec à Montréal, Montreal, Quebec, Canada

^b Research Applications Laboratory, NCAR, Boulder, Colorado

(Manuscript received 15 June 2020, in final form 12 January 2021)

ABSTRACT: The collection efficiency of a typical precipitation gauge-shield configuration decreases with increasing wind speed, with a high scatter for a given wind speed. The high scatter in the collection efficiency for a given wind speed arises in part from the variability in the characteristics of falling snow and atmospheric turbulence. This study uses weighing gauge data collected at the Marshall Field Site near Boulder, Colorado, during the WMO Solid Precipitation Intercomparison Experiment (SPICE). Particle diameter and fall speed data from a laser disdrometer were used to show that the scatter in the collection efficiency can be reduced by considering the fall speed of solid precipitation particles. The collection efficiency was divided into two classes depending on the measured mean-event particle fall speed during precipitation events. Slower-falling particles were associated with a lower collection efficiency. A new transfer function (i.e., the relationship between collection efficiency and other meteorological variables, such as wind speed or air temperature) that includes the fall speed of the hydrometeors was developed. The root-mean-square error of the adjusted precipitation with the new transfer function with respect to a weighing gauge placed in a double fence intercomparison reference was lower than using previously developed transfer functions that only consider wind speed and air temperature. This shows that the measured fall speed of solid precipitation with a laser disdrometer accounts for a large amount of the observed scatter in weighing gauge collection efficiency.

KEYWORDS: Atmosphere; Snowfall; Automatic weather stations; Data processing; Measurements; Surface observations

1. Introduction

Measuring snowfall with a gauge on the ground is prone to many sources of uncertainty. The effect of horizontal wind speed has been identified as the main meteorological factor impacting the collection efficiency (CE) of gauges for solid precipitation (Goodison et al. 1998; Rasmussen et al. 2012). CE is the ratio of the amount of precipitation collected in the gauge shield of interest and the “truth” that is measured by the WMO reference shield/gauge system [double fence intercomparison reference (DFIR)]. While there is a known decrease of CE with increasing horizontal wind speed, it is also found that a large scatter exists for a given wind speed that tends to decrease with increasing wind speed. Most of this scatter is due to the trajectory of snowflakes headed toward a gauge being deflected by the flow field in the vicinity of the gauge. Blowing snow and evaporation (e.g., Rauch et al. 1998; Sevruk 1982, 1996) can vary between the different gauges used (Yang et al. 2001; Rasmussen et al. 2012) and also cause variability.

Yang et al. (1999) showed that CE depends on whether the precipitation is snow, rain, or mixed precipitation. Initial computational fluid dynamics calculations of hydrometeor deflection around gauges solely focused on raindrop collection

(Nešpor and Sevruk 1999). Thériault et al. (2012) demonstrated that the type of snowflakes also impacts the CE. In particular, Thériault et al. (2012) showed through computational fluid dynamics simulations and field measurements of ice crystals that the slower falling snowflakes tend to follow the streamlines and, in turn, are deflected upward by an updraft forming at the edge of the gauge. In contrast, fast-falling snowflakes tend to cross streamlines and enter the gauge. By comparing the numerical simulations with field data of CE variation with wind speed, Thériault et al. (2012) showed that the distribution of particle types falling during a snowfall event can help explain the scatter in CE.

To correct solid precipitation measurements for wind undercatch, transfer functions have been developed; some transfer functions only consider the wind speed (e.g., Smith 2009). Using wind speed transfer function to correct for precipitation undercatch decreases the precipitation bias without changing the scatter in the data, which is quantified by the root-mean-square error (RMSE). Air temperature, which is assumed to be a good proxy for precipitation type diagnostic (e.g., Wolff et al. 2013), is often added as another variable in transfer functions to further reduce the scatter in the data for a given wind speed (e.g., Chubb et al. 2015; Wolff et al. 2015; Kochendorfer et al. 2017a,b, 2018). Chubb et al. (2015) and Colli et al. (2020) used precipitation intensity in addition to wind speed and air temperature to correct precipitation measurements from weighing gauges. Including precipitation intensity further improves both the bias and the scatter in the data compared to using the wind speed and the air temperature alone to correct precipitation measurements.

 Denotes content that is immediately available upon publication as open access.

Corresponding author: Nicolas R. Leroux, leroux.nicolas_roumain@uqam.ca

DOI: 10.1175/JHM-D-20-0147.1

© 2021 American Meteorological Society. For information regarding reuse of this content and general copyright information, consult the AMS Copyright Policy (www.ametsoc.org/PUBSReuseLicenses).

The phase and type of precipitation are often diagnosed using a disdrometer as it measures the size and fall speed of precipitation particles (e.g., Yuter et al. 2006). Video disdrometers have been used to characterize the density, size distribution and fall speed of solid precipitation (e.g., Barthazy and Schefold 2006; Brandes et al. 2007; Ishizaka et al. 2013; Lee et al. 2015; Raupach et al. 2017; Szyrmer and Zawadzki 2010), as well as to diagnose the main type of solid precipitation falling (Ishizaka et al. 2013; Grazioli et al. 2014; Bernauer et al. 2016; Praz et al. 2017). The Multi-Angle Snowflake Camera (MASC; Garrett and Yuter 2014) measures snow particles characteristics with unprecedented detail by taking high-resolution photos of each particle. Laser disdrometers, such as the Thies and Parsivel (e.g., Angulo-Martínez et al. 2018), are a good alternative to video disdrometers but require approximations to be done on the shape, size, and riming degree of the snow particles (Battaglia et al. 2010). Many studies used laser disdrometers to study rain drop distribution (e.g., Angulo-Martínez et al. 2018; Raupach and Berne 2015; Kim and Lee 2016; Chen et al. 2016). Laser disdrometers have also been applied to differentiate between solid and liquid precipitation types (Thériault et al. 2018), as well as to estimate solid precipitation amounts (Zhang et al. 2015).

Given that snowfall measurements using standard weighing gauges are impacted by the precipitation microphysics, it is critical to improve our understanding of the key factors influencing the CE. The objective of this study is to show that the measured solid precipitation particle fall speeds as estimated by a laser disdrometer can contribute to reduce the scatter in the measured snowfall for a given wind speed and can thus be used to improve the transfer functions. To address this, data collected during the World Meteorological Organization Solid Precipitation Intercomparison Experiment (WMO-SPICE; Nitu et al. 2018) from the Marshall Field Site (Rasmussen et al. 2012) are used. In particular, we focused on an unshielded Geonor precipitation gauge, a Geonor precipitation gauge placed in a single-Alter shield, a Geonor in a DFIR shield, as well as particle fall speeds measured by an unshielded laser disdrometer, the OTT Parsivel².

The paper is organized as follows. The methodology is given in section 2. The Parsivel² observations and their relationship to the CE of the shielded and unshielded Geonor precipitation gauges are analyzed in section 3. Section 4 introduces the newly developed transfer functions that include the precipitation particle fall speed and a comparison with previously developed transfer functions. Discussion and conclusions are presented in section 5.

2. Methodology

Solid precipitation and meteorological data collected at the Marshall Field Site in Boulder, Colorado, at an elevation of 1700 m (39.949°N, 105.195°W) (Rasmussen et al. 2012) are analyzed in this study. This midlatitude site is subject to a dry continental climate. This site is on a flat and level terrain with semiarid grasses less than 0.25 m high. A detailed description of the Marshall Field Site is given in Rasmussen et al. (2012) and

Nitu et al. (2018). A description of the datasets and the methodology are given in the next subsections.

a. WMO-SPICE datasets

The data used in this study were collected in 2013–14 and 2014–15 during WMO-SPICE (Nitu et al. 2018) at the Marshall Field Site, Boulder, Colorado. The WMO-SPICE data were divided into 30-min precipitation segments using a strict quality control described in Kochendorfer et al. (2017a,b). The key data used in this study came from the unshielded Geonor (thereafter called UN), a Geonor in a single-Alter (thereafter called SA), Geonor in a DFIR (thereafter called DFIR), and also included the 2-m temperature, and 10-m wind speed and direction. The measurements from the DFIR are assumed to be the true precipitation amount; however, DFIR measurements still present an undercatch of solid precipitation lower than 10% (Yang et al. 1993). The wind speed at gauge height (~2 m) was estimated from the 10-m wind speed using a log-law profile with a roughness length of 1 cm and displacement height of 40 cm following Kochendorfer et al. (2017a). Only solid precipitation events (air temperature < -2°C) were considered to enable us to understand the scatter of the solid precipitation data.

As in Kochendorfer et al. (2017a,b, 2018), the 30-min precipitation events were filtered as follows: 1) events with precipitation measured by the DFIR < 0.25 mm were neglected; 2) events with northerly wind coming from $\pm 30^\circ$ were filtered out due to wind blockage between instruments, as well as with horizontal wind speeds equal to zero; 3) events with horizontal wind speeds at gauge height above 5 m s^{-1} were eliminated due to the low number of samples (~10 events) and to limit the impact of blowing snow on the measurements (Kochendorfer et al. 2017a,b). This data filtering reduced the number of acceptable events to 197 with a mean wind speed of 2.7 m s^{-1} and a mean air temperature of -6.5°C .

b. Disdrometer data

An OTT Parsivel² laser disdrometer sensor was operated at the Marshall Field Site during WMO-SPICE. This instrument measures particle fall speed every one minute and the equivalent volume diameter of the falling hydrometeors in 32 diameter and 32 fall speed bins. The 32 diameter bins cover the range from 0.062 to 24.5 mm (midclass values), while the 32 fall speed bins cover the range between 0.05 and 20.8 m s^{-1} (midclass values).

The disdrometer data were also subject to a strict quality control. First, it was verified that the internal program did not detect a dirty laser protective glass or a damaged laser during the 197 events identified in section 2a. The average of all the 1-min fall speeds within a 30-min event (the mean-event fall speed, denoted by v_m) was computed for each 30-min precipitation event using only the particles with diameters > 1 mm as suggested by Yuter et al. (2006). Third, the events associated with outliers, i.e., with v_m corresponding to z score > 3, were also removed. For the z score computation, the average of all the v_m was 1.26 m s^{-1} and the standard deviation was 0.28 m s^{-1} . This filter removed only two events. Therefore, a total of 195 precipitation events were used in our analysis.

The median of all the v_m was 1.2 m s^{-1} , and this value was used to separate the 195 events into two classes, those with $v_m \leq 1.2 \text{ m s}^{-1}$ and those with $v_m > 1.2 \text{ m s}^{-1}$. For the SA and UN, there were 103 and 92 events in the class $v_m \leq 1.2 \text{ m s}^{-1}$, respectively, whereas there were 92 and 103 events in the class $v_m > 1.2 \text{ m s}^{-1}$, respectively. The number of events in each class differ for SA and UN due to the quality control for each instrument presented in section 2a. The separation of the events into the two classes based on v_m was identical for each instrument. An example of the 1-min fall speeds measured in each diameter bins during a 30-min event and the associated v_m is given in Fig. 1. The empirical diameter–fall speed relationships for dry/unrimed and wet/rimed snow particles from Rasmussen et al. (1999) corrected for elevation are also included in Fig. 1 to illustrate the type of solid precipitation represented in this distribution. Similar patterns were observed for the other events. The dry snow and wet snow particle types are assumed spherical, and their diameters correspond to the volume equivalent diameter measured by the Parsivel². Finally, v_m was compared with the 2-m temperature and the 2-m wind speed and the variability of 1-min fall speeds during each 30-min event was also analyzed.

c. Transfer function models

To assess the added value of using the particle fall speed to improve the bias, the coefficient of determination (R^2), and the RMSE when adjusting solid precipitation measurements, a new transfer function was developed and compared with those proposed by Kochendorfer et al. (2017a,b). Transfer functions estimate the CE, which is the ratio of measured precipitation by a gauge under test to the “true” precipitation measured by a DFIR, as a function of meteorological variables.

A transfer function that includes wind speed was developed for each one of the two classes of events defined in section 2b. Those are the slow-falling particles ($v_m \leq 1.2 \text{ m s}^{-1}$) and fast-falling particles ($v_m > 1.2 \text{ m s}^{-1}$). The form of the transfer function is the same as Kochendorfer et al. (2017b):

$$\text{CE} = (1 - a)e^{-bU}, \quad (1)$$

where a and b are fitting coefficients determined for each class and U is either the 2-m wind speed or the 10-m wind speed (m s^{-1}). Similar to Kochendorfer et al. (2017a, 2018), a tenfold cross validation was used to determine the coefficients a and b for each event class. Through a tenfold cross validation, some independence was preserved between the measurements used for creating the transfer function and those to test the transfer function. During the tenfold cross validation, the fitting model [Eq. (1)] was independently trained in 10 iterations, using 90% of the data of each class to train the model and 10% of the data of each class to test the model. A least squares method was used to determine the best fit. The fitting coefficients of the new transfer function (Table 1) were taken as the average of the coefficients estimated during each of the tenfold cross validations, and the uncertainty of the parameters, i.e., their variability across the 10 iterations, was also evaluated.

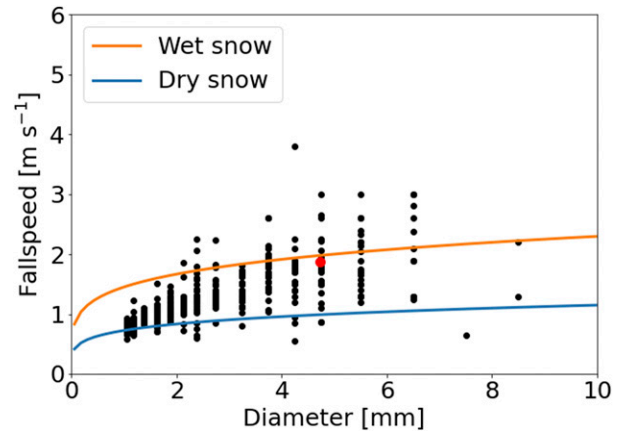


FIG. 1. Example of the measured 1-min fall speeds (dots) by the OTT Parsivel² for one 30-min event. The red dot shows the average of the 1-min fall speeds over the 30-min events, i.e., the mean-event fall speed v_m . The solid lines are the diameter–fall speed relationships for wet snow (orange) and dry snow (blue) hydrometeors (see Rasmussen et al. 1999) and these relationships were corrected for elevation following Heymsfield and Kajikawa (1987). These two particle types are assumed spherical, and their diameters correspond to the volume equivalent diameter measured by the Parsivel². Diameters $< 1 \text{ mm}$ are neglected.

Second, the newly developed transfer function that includes knowledge of the mean-event fall speed [Eq. (1)] is compared with the one developed by Kochendorfer et al. (2017a,b) that includes wind speed and temperature as predictive variables:

$$\text{CE} = \exp\{-\alpha U[1 - \tan^{-1}(\beta T) + \gamma]\} \quad (2)$$

where α , β , and γ are fitting coefficients, U is the 10-m wind speed (m s^{-1}), and T is the 2-m air temperature ($^{\circ}\text{C}$). The fitting coefficients are presented in Kochendorfer et al. (2017b).

Finally, the measured and adjusted precipitation measurements from the SA and the UN are compared to measured precipitation from the DFIR using the RMSE, bias, and R^2 . The RMSE, bias, and R^2 of the adjusted SA and UN using the newly fitted transfer function [Eq. (1)] for each fall speed class was taken as the average values found in each of the 10 iterations for the cross validation.

3. Mean-event particle fall speed (v_m)

The variability of the 1-min fall speeds with particle diameters during a 30-min event is illustrated in Fig. 1, while the range of fall speeds during each 30-min event is shown in Fig. 2. It is evident that most particles fall at velocities $< 1.2 \text{ m s}^{-1}$. Events with $v_m > 1.2 \text{ m s}^{-1}$ are associated with a wider range of fall speeds, reaching up to 2.6 m s^{-1} at the upper end. From Fig. 1, we can approximate that the fall speeds $< 1.2 \text{ m s}^{-1}$ are associated with dry/unrimed snow particles and particles falling faster than 1.2 m s^{-1} are associated with wet snow.

The link between v_m with the 30-min averaged horizontal 2-m wind speed and 2-m air temperature is shown Fig. 3. No

TABLE 1. Fitting coefficients a and b for Eq. (1) with the data presented in Fig. 5. The standard deviation is shown in parentheses; v_m (m s^{-1}) is the average of the measured 1-min fall speeds over a 30-min event.

		Using 2-m wind speed in Eq. (1)		Using 10-m wind speed in Eq. (1)	
		a	b	a	b
UN	$v_m \leq 1.2 \text{ m s}^{-1}$	-0.28 (0.01)	0.44 (0.005)	-0.28 (0.01)	0.32 (0.004)
	$v_m > 1.2 \text{ m s}^{-1}$	-0.20 (0.01)	0.33 (0.005)	-0.20 (0.01)	0.24 (0.004)
SA	$v_m \leq 1.2 \text{ m s}^{-1}$	-0.31 (0.013)	0.27 (0.005)	-0.31 (0.013)	0.20 (0.003)
	$v_m > 1.2 \text{ m s}^{-1}$	-0.27 (0.02)	0.22 (0.006)	-0.27 (0.02)	0.16 (0.005)

clear correlation is found between v_m and the 2-m wind speed (spearman correlation coefficient of 0.33). In contrast, v_m can be somewhat related to the 2-m temperature (spearman correlation coefficient of 0.58) but with a lot of variation for a given temperature. For instance, warmer air temperatures are associated with faster-falling particles, which could be wet/rimed snowflakes, whereas the slower falling particles are associated with colder temperatures, and can be associated with dry/unrimed snowflakes. At around -5°C , v_m can vary between 0.9 and 1.8 m s^{-1} . This degree of variability shows the challenge of using the air temperature as a proxy for solid precipitation types.

4. Impact of v_m on the collection efficiency

The CE values for the unadjusted UN and SA gauges as a function of the 2-m wind speed for the two classes of v_m are shown in Fig. 4. The number of events in each class per wind speed bin is summarized in Table 2. A high number of slow-falling particles are measured at wind speeds $< 3 \text{ m s}^{-1}$. For wind speeds $> 4 \text{ m s}^{-1}$, only a few events are associated with $v_m \leq 1.2 \text{ m s}^{-1}$. Despite the variability of CE at a given wind speed within each class, events with $v_m > 1.2 \text{ m s}^{-1}$ have a higher catch efficiency than those with $v_m \leq 1.2 \text{ m s}^{-1}$ for both UN and SA.

The transfer function to adjust the data based on the measured wind speed [Eq. (1)] was fitted to the data separated in the two classes of v_m . Table 1 presents the fitted coefficients a and b for Eq. (1) using the 10-m wind speed and the 2-m wind speed (gauge height). The standard deviations of the fitted variables using the tenfold cross validation are presented in brackets in Table 1. The best fitted variables were similar for all the 10 iterations, which is shown by small standard deviations ($< 10\%$ of the mean value of the fitted parameters). The newly fitted transfer functions against the 10-m or 2-m wind speed [Eq. (1)] could not be visually differentiated. The best fits against the CE of the unadjusted precipitation measurements are presented in Fig. 5. For SA, a wider spread of the unadjusted data per class is visible, particularly for higher wind speeds. This scatter in the observations resulted in uncertainties in the fitted transfer functions at high wind speeds.

The “true” precipitation measurements by the DFIR were compared to the uncorrected precipitation measurements (Figs. 6a,d) and adjusted precipitation measurements from SA and UN (Figs. 6b,c,e,f). The adjusted measurements using the transfer function from Kochendorfer et al. (2017a,b) [Figs. 6b,e, subscript $f(U, T)$] remained mainly underestimated compared to the DFIR measurements. On the other hand, the adjusted measurements with the newly developed transfer function based on the mean-event fall speed

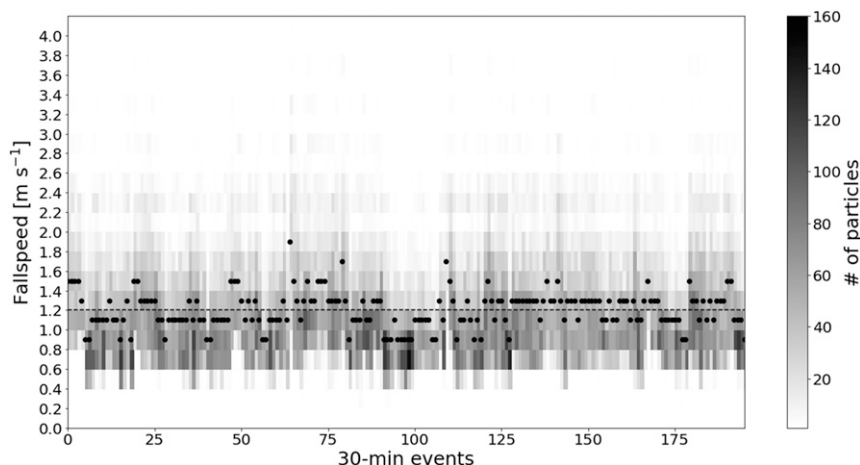


FIG. 2. Distribution of the measured 1-min fall speed in 0.2 m s^{-1} bins per 30-min precipitation event. The gray scale presents the number of particles in each 0.2 m s^{-1} bin. The mean-event fall speeds v_m are represented by the dots. The dotted line shows the 1.2 m s^{-1} mean-event fall speed threshold used to separate the precipitation events into two classes.

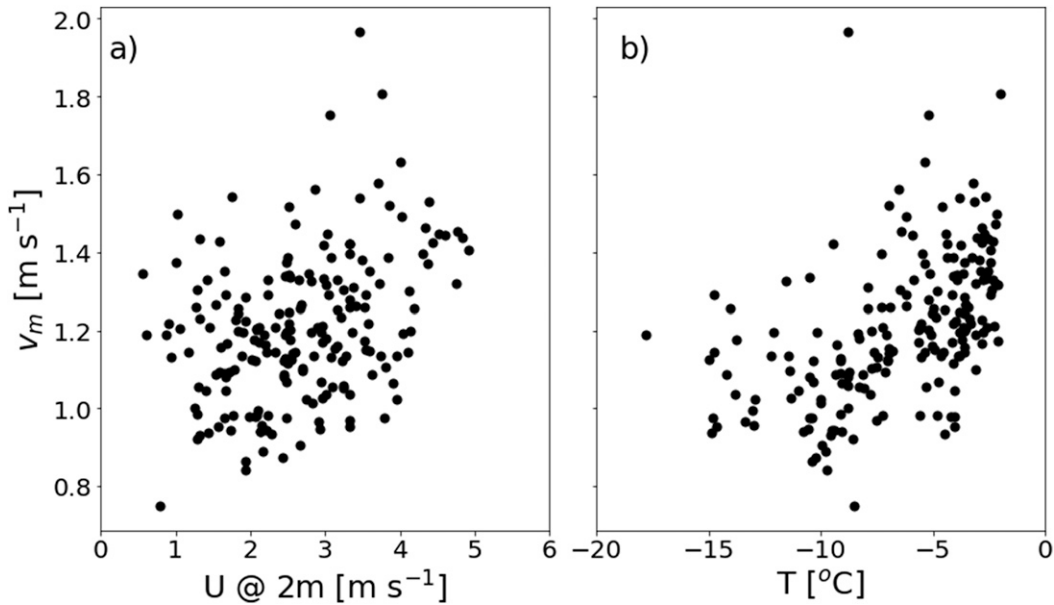


FIG. 3. Variation of the mean-event fall speeds v_m with (a) the wind speed at 2 m above the ground and (b) with the air temperature at 2 m.

followed more closely the DFIR measurements [Figs. 6c,f, subscript $f(U, v_m)$].

The comparison of the accumulated solid precipitation during a 30-min event shown in Fig. 6 is summarized in Fig. 7. All methods produced a negative bias in the 30-min precipitation accumulation. The bias improved when both the wind speed and temperature are used to correct the measurements and is near 0 mm when the mean fall speed consideration is accounted for in the transfer function.

This can also be seen in Fig. 8, where the total accumulated precipitation using the unadjusted data as well as the adjusted data are shown. The corrected measurements with the new transfer function resulted in an excellent estimation of the accumulated precipitation across all the events. Note that the RMSE decreased when considering the mean-event fall speed for both UN and SA and R^2 also improved. This indicates that not only the total amount of adjusted precipitation improved but also the scatter of the

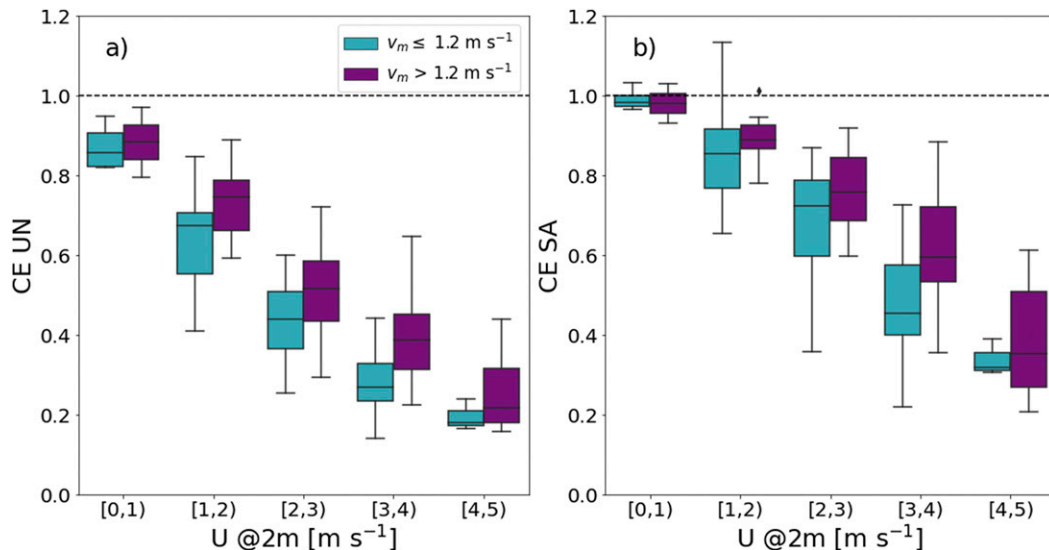


FIG. 4. Variation of the collection efficiency (CE) as a function of the 2-m wind speed for (a) the unshielded gauge (UN) and (b) the gauge placed in a single-Altair shield (SA) as a function of the mean-event fall speed v_m above and below 1.2 m s^{-1} . Here, $[0,1)$ means ≥ 0 and $< 1 \text{ m s}^{-1}$.

TABLE 2. Number of samples for each wind speed bin for each class of mean-event particle fall speed ($v_m \leq 1.2 \text{ m s}^{-1}$ and $v_m > 1.2 \text{ m s}^{-1}$) for each instrument. The wind speed interval [0, 1) means $\geq 0 \text{ m s}^{-1}$ and $< 1 \text{ m s}^{-1}$.

2-m wind speed (m s^{-1})	Single-Alter shielded Geonor gauge (SA)		Unshielded Geonor gauge (UN)	
	$v_m \leq 1.2 \text{ m s}^{-1}$	$v_m > 1.2 \text{ m s}^{-1}$	$v_m \leq 1.2 \text{ m s}^{-1}$	$v_m > 1.2 \text{ m s}^{-1}$
[0, 1)	4	2	4	2
[1, 2)	27	19	27	19
[2, 3)	45	28	45	28
[3, 4)	24	28	22	28
[4, 5)	3	15	3	17

data was reduced when considering the measured mean-event particle fall speed.

5. Summary and conclusions

a. Summary

Hydrometeor characteristics, such as fall speed and diameter, measured with a laser disdrometer, were used to investigate the scatter in collection efficiency (CE) as a function of wind speed for two instruments: an unshielded Geonor precipitation gauge (UN) and a Geonor precipitation gauge in a single-Alter shield (SA).

The assumptions, limitations, and uncertainties of this study can be summarized as follows:

- Only solid precipitation was considered ($T < -2^\circ\text{C}$).
- The maximum wind speed measured during those events was 5 m s^{-1} .
- 30-min events were analyzed.
- The OTT Parsivel² was unshielded.
- Only particles with volume equivalent diameters $> 1 \text{ mm}$ were considered.
- Known limitations of using a laser disdrometer to measure solid precipitation (Battaglia et al. 2010).
- Data from one site were analyzed. The site is subject to a dry continental climate and has a vegetation corresponding to semiarid grasses $< 0.25 \text{ m}$.

- The precipitation amounts and particle fall speeds were measured at 2 m (gauge height) above the ground.

To apply this methodology at other sites, the recommendations from the WMO-SPICE experiment should be followed (Nitu et al. 2018), as well as the quality control from Kochendorfer et al. (2017a,b). For instance, wind speed and direction should be measured at gauge height or at 10 m above the ground and air temperature measured at 2 m above the ground. Such measurements are already widely done, for instance at the SNOTEL sites. This study could be used at other site elevations because field measurements of particle fall speeds were used instead of particle types, as the empirical fall speed–diameter equation for a particle type needs to be adjusted for elevation change (e.g., Heymsfield and Kajikawa 1987).

The measured fall speed at 1-min interval with the Parsivel² allowed for the estimation of a mean fall speed for each 30-min event (v_m). The analysis presented in this paper used v_m to reduce the scatter in CE at a given wind speed. A low correlation between air temperature and v_m suggests that the temperature may not be a good proxy to diagnose ice crystal types at the Marshall Field Site. The low correlation between wind speed and v_m suggests little impact of the wind speed on the fall speed of hydrometeors. The poor correlation with temperature can be anticipated as the presence of fast-falling rimed particles (Thériault et al. 2012) is

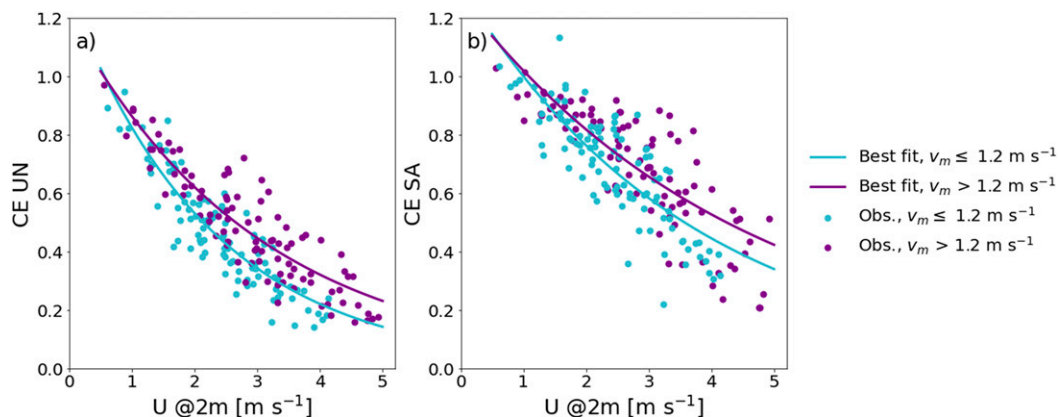


FIG. 5. CE as a function of the 2-m wind speed for 30-min mean fall speeds $v_m > 1.2 \text{ m s}^{-1}$ (magenta dots) and for 30-min mean fall speeds $\leq 1.2 \text{ m s}^{-1}$ (cyan dots) for (a) UN precipitation measurements and (b) SA precipitation measurements. The lines present the best fits using Eq. (1) and a least squares method.

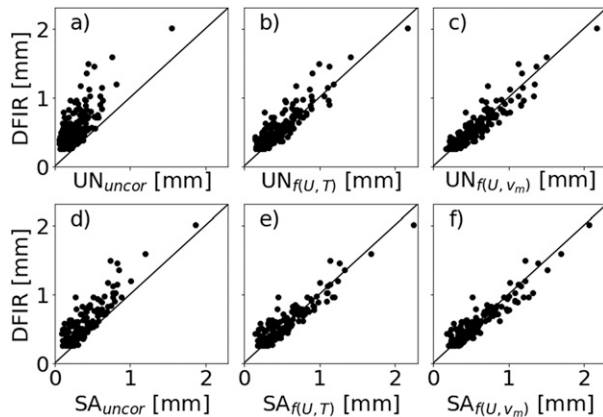


FIG. 6. Comparison of 30-min precipitation measurements from the DFIR against (a) the unadjusted UN precipitation measurements and (b),(c) adjusted UN precipitation measurements and (d) unadjusted SA precipitation measurements and (e),(f) adjusted SA precipitation measurements. The precipitation adjustments in (b) and (e) are done using both the 10-m wind speed and the 2-m air temperature [subscript $f(U, T)$], and precipitation adjustments in (c) and (f) are corrected using the 10-m wind speed and for both classes of v_m [subscript $f(U, v_m)$].

most common at temperatures $> -12^{\circ}\text{C}$ (Kneifel and Moissev 2020). Therefore, it is difficult to differentiate dry snow and wet/rimed snow based only on 2-m air temperature given the range of temperature in which riming can occur.

A threshold of 1.2 m s^{-1} for v_m was used to classify the events into two categories. This threshold corresponded to the median of all the v_m . Events with $v_m > 1.2\text{ m s}^{-1}$ have higher catch efficiencies than those $\leq 1.2\text{ m s}^{-1}$. The results of this study were not sensitive to small variations of this threshold ($1.2 \pm 0.2\text{ m s}^{-1}$), i.e., the biases, RMSE, and R^2 were still greatly improved with thresholds of $1.2 \pm 0.2\text{ m s}^{-1}$ using the new method. Faster-falling particles are less affected by the wind

speed and the turbulence around the gauge, resulting in a higher CE.

The fall speed can be linked to solid precipitation particles type. As shown in Fig. 1, faster-falling particles are associated with wet/rimed snow and slower-falling ones with dry snow. Dry snow are more affected by the deflection of the wind around the gauge than fast-falling particles, such as wet snow/rimed snow. This is in accordance with previous studies on the impact of wind speed and turbulence effects around a Geonor gauge on particle trajectory using computational fluid dynamics models (Thériault et al. 2012; Colli et al. 2015a,b), as well with the field observations of ice crystals conducted by Thériault et al. (2012).

A simple transfer function that only requires the measured wind speed was fitted to the CE for each class of events based on the mean-event fall speed for each gauge. To use this function, the mean particle fall speed during the 30-min events needs to be determined first, and then Eq. (1) can be applied with the fitting coefficients in Table 1 based on the class in which the event belongs. The transfer function presented here may not be universal as it was determined from measurements at one site only with chosen restrictions (2-m wind speeds $< 5\text{ m s}^{-1}$ and air temperatures $< -2^{\circ}\text{C}$); however, the fundamental findings of our study are in accordance with Thériault et al. (2012) and Colli et al. (2015a,b) that suggest that the undercatch is closely related to the fall speed and the updraft upstream of the gauge. It should be noted that the site chosen for the evaluation was a fairly typical midlatitude site in that the temperature, wind speed, and snowfall rate when considered average compared to the worldwide dataset collected by the SPICE project. It should also be noted that a tenfold cross validation was used to have some independence between the measurements used for developing and those for evaluating the transfer function.

Future studies should evaluate this approach at other sites with a wider range of wind and precipitation conditions. Adjusting the precipitation measurements by the newly fitted

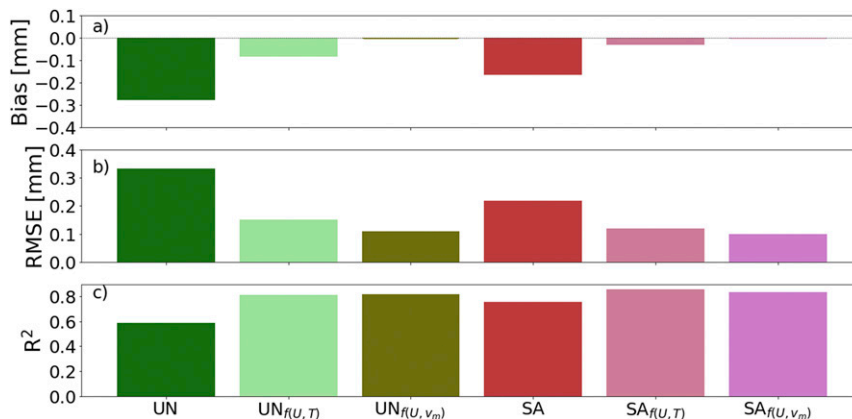


FIG. 7. (a) Bias, (b) RMSE, and (c) R^2 between the 30-min DFIR data and the unadjusted and adjusted SA and UN measurements. The measurements adjusted using both the 10-m wind speed and the 2-m air temperature have the subscript $f(U, T)$ and those corrected using the 10-m wind speed and for both mean-event particle fall speed classes of are denoted with $f(U, v_m)$.

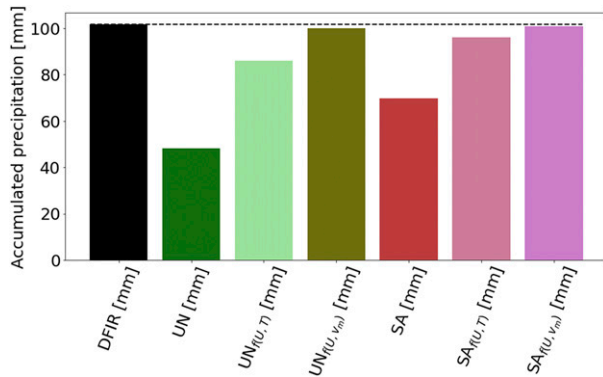


FIG. 8. Total accumulated precipitation of all the events measured by the DFIR, the unadjusted and adjusted SA and UN measurements. The subscript $f(U, T)$ means that the UN and SA measurements were adjusted using the 10-m wind speed and the 2-m air temperature. The subscript $f(U, v_m)$ means that the UN and SA measurements were adjusted using the 10-m wind speed based on the class of v_m . The dashed line shows the accumulated precipitation measured by the Geonor precipitation gauge in the DFIR.

transfer function resulted in radically reduced RMSE (reduced by half for SA and by 2/3 for UN) compared to unadjusted measurements and a zero bias. These results are of particular importance for the unshielded Geonor precipitation gauge, for which adjusted precipitation produced with the current approach were similar to those of the single-Alter Geonor precipitation gauge. It can be noted that the undercatch of the unadjusted precipitation measurements of the unshielded gauge at low wind speeds ($<1 \text{ m s}^{-1}$) was improved by the new method as well. This means that improved precipitation measurements can be obtained by having an OTT Parsivel² or other instrument measuring the fall speed of particles collocated with precipitation gauge.

b. Conclusions

This study highlighted the impact of the solid precipitation fall speed on the collection efficiency of an unshielded and shielded Geonor precipitation gauges. The key concluding remarks are as follows.

- The precipitation particle fall speed varies within a 30-min event as well as from event to event.
- Higher collection efficiencies were observed for faster-falling particles ($>1.2 \text{ m s}^{-1}$). In contrast, lower collection efficiencies were mostly associated with slower-falling particles ($\leq 1.2 \text{ m s}^{-1}$).
- A new method to adjust solid precipitation that includes knowledge of measured particle fall speeds was developed for both unshielded and shielded Geonor precipitation gauges. It improved the bias to close to 0 mm compared to other methods using winds speed and temperature.
- The use of the precipitation particle fall speed for adjusting precipitation measurements in addition to horizontal wind speed reduced the scatter in the data. The RMSE was decreased by $\sim 50\%$ for the Geonor precipitation gauge in

the single-Alter shield and by $\sim 66\%$ for the unshielded Geonor precipitation gauge.

This study has some limitations and uncertainties. For this study, the wind speed at gauge height was limited to 5 m s^{-1} to reduce the uncertainties caused by processes occurring at high wind speed and the relatively few data points at higher wind speeds. Future studies using data from high wind sites may alleviate this problem. Particles with diameters lower than 1 mm were disregarded in this study based on recommendations from previous studies with laser disdrometers. Additional work could help better understand the limitations of using an laser disdrometer to measure solid precipitation.

Finally, some errors remain and ideally a precipitation gauge that reduces the distortion of the flow through which snowflakes pass will perform better. The hotplate precipitation gauge (Rasmussen et al. 2011) would be ideal in this sense as it presents an aerodynamic profile to the oncoming flow (Cauteruccio 2020; Thériault et al. 2021).

Acknowledgments. The research was funded by the Natural Sciences and Engineering Research Council of Canada (NSERC) Discovery Grant, the Canadian Research Chair Tier 2 and the NCAR Water System Program. The authors thank Scott Landolt, Joshua Lave, and John Kochendorfer for sharing the data as well as Matteo Colli and Luca G. Lanza for previous discussion.

Data availability statement. Data from the Marshall Field Site are available in the supplement file provided with Colli et al. (2020). OTT Parsivel² data are available upon request to the Research Applications Laboratory (RAL) of the National Center for Atmospheric Research (NCAR).

REFERENCES

- Angulo-Martínez, M., S. Beguería, B. Latorre, and M. Fernández-Raga, 2018: Comparison of precipitation measurements by OTT Parsivel² and Thies LPM optical disdrometers. *Hydrol. Earth Syst. Sci.*, **22**, 2811–2837, <https://doi.org/10.5194/hess-22-2811-2018>.
- Barthazy, E., and R. Schefold, 2006: Fall velocity of snowflakes of different riming degree and crystal types. *Atmos. Res.*, **82**, 391–398, <https://doi.org/10.1016/j.atmosres.2005.12.009>.
- Battaglia, A., E. Rustemeier, A. Tokay, U. Blahak, and C. Simmer, 2010: PARSIVEL snow observations: A critical assessment. *J. Atmos. Oceanic Technol.*, **27**, 333–344, <https://doi.org/10.1175/2009JTECHA1332.1>.
- Bernauer, F., K. Hürkamp, W. Rühm, and J. Tschiersch, 2016: Snow event classification with a 2D video disdrometer - A decision tree approach. *Atmos. Res.*, **172–173**, 186–195, <https://doi.org/10.1016/j.atmosres.2016.01.001>.
- Brandes, E. A., K. Ikeda, G. Zhang, M. Schönhuber, and R. M. Rasmussen, 2007: A statistical and physical description of hydrometeor distributions in Colorado snowstorms using a video disdrometer. *J. Appl. Meteor. Climatol.*, **46**, 634–650, <https://doi.org/10.1175/JAM2489.1>.
- Cauteruccio, A., 2020: The role of turbulence in particle-fluid interaction as induced by the outer geometry of catching-type precipitation gauges. Ph.D. thesis, University of

- Genoa, 176 pp., https://doi.org/10.15167/cauteruccio-arianna_phd2020-04-06.
- Chen, B., J. Wang, and D. Gong, 2016: Raindrop size distribution in a midlatitude continental squall line measured by Thies optical disdrometers over East China. *J. Appl. Meteor. Climatol.*, **55**, 621–634, <https://doi.org/10.1175/JAMC-D-15-0127.1>.
- Chubb, T., M. J. Manton, S. T. Siems, A. D. Peace, and S. P. Bilish, 2015: Estimation of wind-induced losses from a precipitation gauge network in the Australian snowy mountains. *J. Hydrometeorol.*, **16**, 2619–2638, <https://doi.org/10.1175/JHM-D-14-0216.1>.
- Colli, M., L. G. Lanza, R. Rasmussen, and J. M. Thériault, 2015a: The collection efficiency of shielded and unshielded precipitation gauges. Part I: CFD airflow modeling. *J. Hydrometeorol.*, **17**, 231–243, <https://doi.org/10.1175/JHM-D-15-0010.1>.
- , —, —, and —, 2015b: The collection efficiency of shielded and unshielded precipitation gauges. Part II: Modeling particle trajectories. *J. Hydrometeorol.*, **17**, 245–255, <https://doi.org/10.1175/JHM-D-15-0011.1>.
- , M. Stagnaro, L. G. Lanza, R. Rasmussen, and J. M. Thériault, 2020: Adjustments for wind-induced undercatch in snowfall measurements based on precipitation intensity. *J. Hydrometeorol.*, **21**, 1039–1050, <https://doi.org/10.1175/JHM-D-19-0222.1>.
- Garrett, T. J., and S. E. Yuter, 2014: Observed influence of riming, temperature, and turbulence on the fallspeed of solid precipitation. *Geophys. Res. Lett.*, **41**, 6515–6522, <https://doi.org/10.1002/2014GL061016>.
- Goodison, B., P. Louie, and D. Yang, 1998: WMO solid precipitation measurement intercomparison: Final Report. WMO Tech. Doc. 872, 211 pp.
- Grazioli, J., D. Tuia, S. Monhart, M. Schneebeli, T. Raupach, and A. Berne, 2014: Hydrometeor classification from two-dimensional video disdrometer data. *Atmos. Meas. Tech.*, **7**, 2869–2882, <https://doi.org/10.5194/amt-7-2869-2014>.
- Heymsfield, A. J., and M. Kajikawa, 1987: An improved approach to calculating terminal velocities of plate-like crystals and graupel. *J. Atmos. Sci.*, **44**, 1088–1099, [https://doi.org/10.1175/1520-0469\(1987\)044<1088:AIATCT>2.0.CO;2](https://doi.org/10.1175/1520-0469(1987)044<1088:AIATCT>2.0.CO;2).
- Ishizaka, M., H. Motoyoshi, S. Nakai, T. Shiina, T. Kumakura, and K. Muramoto, 2013: A new method for identifying the main type of solid hydrometeors contributing to snowfall from measured size-fall speed relationship. *J. Meteor. Soc. Japan*, **91**, 747–762, <https://doi.org/10.2151/jmsj.2013-602>.
- Kim, D.-K., and D.-I. Lee, 2016: Raindrop size distribution properties associated with vertical air motion in the stratiform region of a springtime rain event from 1290 MHz wind profiler, micro rain radar and Parsivel disdrometer measurements. *Met. Appl.*, **23**, 40–49, <https://doi.org/10.1002/met.1518>.
- Kneifel, S., and D. Moisseev, 2020: Long-term statistics of riming in nonconvective clouds derived from ground-based Doppler cloud radar observations. *J. Atmos. Sci.*, **77**, 3495–3508, <https://doi.org/10.1175/JAS-D-20-0007.1>.
- Kochendorfer, J., and Coauthors, 2017a: The quantification and correction of wind-induced precipitation measurement errors. *Hydrol. Earth Syst. Sci.*, **21**, 1973–1989, <https://doi.org/10.5194/hess-21-1973-2017>.
- , and Coauthors, 2017b: Analysis of single-Alter-shielded and unshielded measurements of mixed and solid precipitation from WMO-SPICE. *Hydrol. Earth Syst. Sci.*, **21**, 3525–3542, <https://doi.org/10.5194/hess-21-3525-2017>.
- , and Coauthors, 2018: Testing and development of transfer functions for weighing precipitation gauges in WMO-SPICE. *Hydrol. Earth Syst. Sci.*, **22**, 1437–1452, <https://doi.org/10.5194/hess-22-1437-2018>.
- Lee, J., S. Jung, H. Park, S. Kwon, P. Lin, and G. Lee, 2015: Classification of precipitation types using fall velocity-diameter relationships from 2D-video disdrometer measurements. *Adv. Atmos. Sci.*, **32**, 1277–1290, <https://doi.org/10.1007/s00376-015-4234-4>.
- Nešpor, V., and B. Sevruk, 1999: Estimation of wind-induced error of rainfall gauge measurements using a numerical simulation. *J. Atmos. Oceanic Technol.*, **16**, 450–464, [https://doi.org/10.1175/1520-0426\(1999\)016<0450:EOWIEO>2.0.CO;2](https://doi.org/10.1175/1520-0426(1999)016<0450:EOWIEO>2.0.CO;2).
- Nitu, R., and Coauthors, 2018: WMO Solid Precipitation Intercomparison Experiment (SPICE) (2012–2015). Instruments and Observing Methods Rep. 131, 1445 pp., https://library.wmo.int/doc_num.php?explnum_id=5686.
- Praz, C., Y.-A. Roulet, and A. Berne, 2017: Solid hydrometeor classification and riming degree estimation from pictures collected with a Multi-Angle Snowflake Camera. *Atmos. Meas. Tech.*, **10**, 1335–1357, <https://doi.org/10.5194/amt-10-1335-2017>.
- Rasmussen, R. M., J. Vivekanandan, J. Cole, B. Meyers, and C. Masters, 1999: The estimation of snowfall rate using visibility. *J. Appl. Meteor.*, **38**, 1542–1563, [https://doi.org/10.1175/1520-0450\(1999\)038<1542:TEOSRU>2.0.CO;2](https://doi.org/10.1175/1520-0450(1999)038<1542:TEOSRU>2.0.CO;2).
- , J. Hallett, R. Purcell, S. D. Landolt, and J. Cole, 2011: The hotplate precipitation gauge. *J. Atmos. Oceanic Technol.*, **28**, 148–164, <https://doi.org/10.1175/2010JTECHA1375.1>.
- Rasmussen, R., and Coauthors, 2012: How well are we measuring snow: The NOAA/FAA/NCAR winter precipitation test bed. *Bull. Amer. Meteor. Soc.*, **93**, 811–829, <https://doi.org/10.1175/BAMS-D-11-00052.1>.
- Rauch, W., N. Thurner, and P. Harremoes, 1998: Required accuracy of rainfall data for integrated urban drainage modeling. *Water Sci. Technol.*, **37**, 81–89, <https://doi.org/10.2166/wst.1998.0441>.
- Raupach, T. H., and A. Berne, 2015: Correction of raindrop size distributions measured by Parsivel disdrometers, using a two-dimensional video disdrometer as a reference. *Atmos. Meas. Tech.*, **8**, 343–365, <https://doi.org/10.5194/amt-8-343-2015>.
- , A. Gires, I. Tchiguirinskaia, D. Schertzer, and A. Berne, 2017: Multifractional analysis of snowfall recorded using a 2D video disdrometer. *J. Hydrometeorol.*, **18**, 2453–2468, <https://doi.org/10.1175/JHM-D-16-0224.1>.
- Sevruk, B., 1982: Methods of correction for systematic error in point precipitation measurement for operational use. Operational Hydrology Rep. 21, WMO Rep. 589, 91 pp., https://library.wmo.int/doc_num.php?explnum_id=1238.
- , 1996: Adjustment of tipping-bucket precipitation gauge measurements. *Atmos. Res.*, **42**, 237–246, [https://doi.org/10.1016/0169-8095\(95\)00066-6](https://doi.org/10.1016/0169-8095(95)00066-6).
- Smith, C. D., 2009: The relationship between snowfall catch efficiency and wind speed for the Geonor T-200B precipitation gauge utilizing various wind shield configurations. *Proc. 77th Western Snow Conf.*, Canmore, AB, Canada, Western Snow Conference, 115–121, <https://westernsnowconference.org/sites/westernsnowconference.org/PDFs/2009SmithSnowfall.pdf>.
- Szyrmer, W., and I. Zawadzki, 2010: Snow studies. Part II: Average relationship between mass of snowflakes and their terminal fall velocity. *J. Atmos. Sci.*, **67**, 3319–3335, <https://doi.org/10.1175/2010JAS3390.1>.
- Thériault, J. M., R. Rasmussen, K. Ikeda, and S. Landolt, 2012: Dependence of snow gauge collection efficiency on snowflake

- characteristics. *J. Appl. Meteor. Climatol.*, **51**, 745–762, <https://doi.org/10.1175/JAMC-D-11-01116.1>.
- , I. Hung, P. Vaquer, R. E. Stewart, and J. W. Pomeroy, 2018: Precipitation characteristics and associated weather conditions on the eastern slopes of the Canadian Rockies during March–April 2015. *Hydrol. Earth Syst. Sci.*, **22**, 4491–4512, <https://doi.org/10.5194/hess-22-4491-2018>.
- , N. R. Leroux, and R. Rasmussen, 2021: Improvement of solid precipitation measurements using a Hotplate precipitation gauge. *J. Hydrometeorol.*, **22**, 877–885, <https://doi.org/10.1175/JHM-D-20-0168.1>.
- Wolff, M., K. Isaksen, R. Brækkan, E. Alfnes, A. Petersen-Øverleir, and E. Ruud, 2013: Measurements of wind-induced loss of solid precipitation: Description of a Norwegian field study. *Hydrol. Res.*, **44**, 35–43, <https://doi.org/10.2166/nh.2012.166>.
- Wolff, M. A., K. Isaksen, A. Petersen-Øverleir, K. Ødemark, T. Reitan, and R. Brækkan, 2015: Derivation of a new continuous adjustment function for correcting wind-induced loss of solid precipitation: Results of a Norwegian field study. *Hydrol. Earth Syst. Sci.*, **19**, 951–967, <https://doi.org/10.5194/hess-19-951-2015>.
- Yang, D., J. R. Metcalfe, B. E. Goodison, and E. Mekis, 1993: “True snowfall”: An evaluation of the double fence intercomparison reference gauge. *Proc. 50th Eastern Snow Conf./61st Western Snow Conf.*, Quebec City, QC, Canada, Western Snow Conference, 105–111, <https://westernsnowconference.org/node/554>.
- , and Coauthors, 1999: Quantification of precipitation measurement discontinuity induced by wind shields on national gauges. *Water Resour. Res.*, **35**, 491–508, <https://doi.org/10.1029/1998WR900042>.
- , and Coauthors, 2001: Compatibility evaluation of national precipitation gage measurements. *J. Geophys. Res.*, **106**, 1481–1491, <https://doi.org/10.1029/2000JD900612>.
- Yuter, S. E., D. E. Kingsmill, L. B. Nance, and M. Löffler-Mang, 2006: Observations of precipitation size and fall speed characteristics within coexisting rain and wet snow. *J. Appl. Meteor. Climatol.*, **45**, 1450–1464, <https://doi.org/10.1175/JAM2406.1>.
- Zhang, L., L. Zhao, C. Xie, G. Liu, L. Gao, Y. Xiao, and Y. Qiao, 2015: Intercomparison of solid precipitation derived from the weighting rain gauge and optical instruments in the interior Qinghai-Tibetan plateau. *Adv. Meteor.*, **2015**, 936724, <https://doi.org/10.1155/2015/936724>.